Journal of Computer-Aided Molecular Design, 8 (1994) 389–404
ESCOM

J-CAMD 249

Active-site mobility inhibits reductive dehalogenation of 1,1,1-trichloroethane by cytochrome P450cam

Mark D. Paulsen and Rick L. Ornstein*

Molecular Science Research Center, Pacific Northwest Laboratory, Battelle Memorial Institute, P.O. Box 999, Richland, WA 99352, U.S.A.

Received 22 July 1993
Accepted 4 February 1994

Key words: Hexachloroethane; Biodegradation; Molecular dynamics; Enzyme simulation; Protein dynamics

SUMMARY

Recent studies by Wackett and co-workers have shown that cytochrome P450cam is capable of reductively dehalogenating hexachloroethane at a significant rate, but that no appreciable dehalogenation of 1,1,1-trichloroethane is observed. A growing body of evidence indicates that differences in intrinsic reactivity can not completely explain this observation. We therefore explored the possible role of differences in preferred binding orientation and in active-site mobility. A detailed analysis of molecular dynamics trajectories with each of these substrates bound at the active site of P450cam is presented. While the dynamics and overall time-average structure calculated for the protein are similar in the two trajectories, the two substrates behave quite differently. The smaller substrate, 1,1,1-trichloroethane, is significantly more mobile than hexachloroethane and has a preferred orientation in which the substituted carbon is generally far from the heme iron. In contrast, for hexachloroethane, one of the chlorine atoms is nearly always in van der Waals contact with the heme iron, which should favor the initial electron transfer step.

INTRODUCTION

In a 1992 report on contaminants, measured at 91 waste sites at 18 U.S. Department of Energy (DOE) facilities within the weapons complex, halogenated hydrocarbon solvents were found to be one of the most often occurring contaminant classes. Multihalogenated ethylenes and ethanes were among the most prevalent and highest concentrated contaminants of this class occurring in ground water and soils/sediments [1], where compounds have been observed to reach concentrations in excess of two million times U.S. EPA guidelines. Many other government facilities, as well as industrial sites, have serious problems with halogenated solvents, similar to those at DOE sites. Thus, great effort is currently being expended to discover and characterize microbial systems capable of degrading these small, highly halogenated compounds in a timely manner.

*To whom correspondence should be addressed.

One class of enzymes capable of dehalogenating halogenated solvents is the cytochromes P450. Cytochrome P450 enzymes have two major functions: (i) some isozymes have critical and specific roles in metabolism of endogenous substances (i.e., conversion of cholesterol to corticoid and sex hormones); and (ii) other isozymes process the burden of xenobiotic compounds in a relatively nonselective manner (Ref. 2 and references cited therein). The known substrates of P450s range in size from ethylene to cyclosporin A (molecular weight of 1201 Da) [2]. This isozyme class may catalyze the widest variety of reactions of any known enzyme [3]. The superfamily of cytochromes P450 metabolizes a plethora of substrates with an amazing variety of chemical reactions, including hydroxylation of carbon and heteroatoms, dealkylation of amines and ethers and epoxidation of double bonds [4]. The type of reaction being performed depends largely upon the nature and mobility of the substrate [5]. Common to most of these reactions is the formation of a, still hypothetical, iron–oxo intermediate that is stabilized by the axial thiolate ligand.

Although the vast majority of P450-mediated reactions are oxidative, under anaerobic reducing conditions cytochromes P450 have also been shown to be capable of reductively dehalogenating a variety of heavily halogenated hydrocarbons [6,7]. Numerous in vivo studies indicate that cytochromes P450 play a role in biodehalogenation [8–13]. Recently, the dehalogenation of a number of chlorinated methanes [14] and ethanes [15] has been studied in cell cultures of *Pseudomonas putida* and in purified reconstituted cytochrome P450cam systems. Cytochrome P450cam was found to be capable of dehalogenating several heavily halogenated ethanes at rates which, while significantly lower than those seen for its native hydroxylation reactions, were comparable to dehalogenation rates reported for anaerobic cell cultures.

Cytochrome P450cam catalyzes the hydroxylation of camphor to 5-*exo*-hydroxycamphor as the first step in the use of camphor as a carbon and energy source. In order to uncover structure–function–dynamics relationships, it is an excellent system because of the wealth of thermodynamic, kinetic, structural and mutagenic data available for this enzyme [16]. Extensive studies have been reported on the kinetics and thermodynamics of the early steps in the reaction cycle, including substrate binding and electron transfer. Over the last several years, crystal structures have been reported for the substrate-free, camphor-bound and CO–camphor–P450 ternary complexes, as well as for several substrate analogs bound in the active site [17]. In addition, several theoretical studies on the hydroxylation of camphor and various alternate substrates have been published [18–24]. The effect of several active-site mutations on the hydroxylation of different substrates has also been reported [25–27].

The binding of a variety of substrates in the active site of P450cam has been studied using both molecular mechanics and molecular dynamics. Previous studies have generally focused on P450-catalyzed oxidations. Calculations have been performed on models of both the binary complex and the ferryl oxygen intermediate. The results of these simulations have been used to interpret or predict regio- and/or stereospecificity of the product(s) formed. In addition, some of these studies have also addressed coupling between NADH consumption and product formation. For the native substrates, virtually all the NADH consumed in the reaction can be accounted for by alcohol formation. However, for a number of nonnative substrates, a significant fraction of the NADH consumed is lost to formation of hydrogen peroxide and water. For the native substrate, camphor, the simulations show only a single orientation and low mobility, consistent with the experimentally determined product profile and coupling [18]. On the other hand, high mobility is observed for smaller substrates like norcamphor, ethylbenzene and β-methyl styrene,

indicating multiple products [18,20,22]. In addition, trajectories of these more mobile substrates give preferred orientations which indicate low coupling of product formation to NADH consumption, also in agreement with experiment. We wanted to determine whether similar correlations would be seen between reactivity and substrate dynamics for the reductive dechlorination of halogenated ethanes.

In the studies by Wackett and co-workers, significant rates of dechlorination were observed for hexachloroethane, but no dechlorination was observed for 1,1,1-trichloroethane [15]. In an effort to assess the possible contribution of substrate mobility and binding orientation to the different reactivities of these two haloalkanes, we have used molecular dynamics simulations to compare the behavior of the two molecules bound in the active site of cytochrome P450cam. We find that the preferred orientation for the binding of hexachloroethane is consistent with its relatively high activity, while 1,1,1-trichloroethane adopts a conformation in which the substituted carbon has rotated and translated away from the heme iron, which should disfavor the initial electron transfer step. In addition, the calculated mobility of 1,1,1-trichloroethane, bound at the active site, is significantly higher than that of hexachloroethane. Preliminary experiments have been performed to assess the reactivity of 1,1,1-trichloroethane in a nonenzymatic system. These experiments show a slow but measurable rate of dechlorination of 1,1,1-trichloroethane in the presence of free hematin, an Fe(II)-porphyrin complex (L.P. Wackett, unpublished data). This suggests that the lack of any measurable conversion of 1,1,1-trichloroethane in the presence of cytochrome P450cam is not due solely to an inherent lack of reactivity, which is consistent with our calculations. Thus, the lack of dehalogenation of 1,1,1-trichloroethane appears to arise from steric and dynamic causes, rather than solely a lack of inherent chemical reactivity. Studies are underway to test this hypothesis by appropriate active-site redesign.

METHODS

The system for which trajectories were calculated included residues 10–414 of cytochrome P450cam, the heme moiety at the active site, a bound substrate (hexachloroethane or 1,1,1-trichloroethane), 204 crystallographically determined solvent molecules, and a 3 Å layer of explicit solvent, bringing the total number of solvent molecules to 890. The crystallographic structure of camphor-bound P450cam, determined by Poulos and co-workers [28] and obtained from the Protein Data Bank (entry 2CPP), served as the starting point for the simulations [29]. Several recent studies suggest that use of a modest solvation shell can give reasonable results for many properties of interest, while greatly reducing the computational resources required [30,31]. X-ray crystallographic [28] and spectroscopic [32] studies suggest that solvent molecule 515 is a tightly bound cation which activates the enzyme; it was modeled as a sodium ion. The substrates, hexachloroethane or 1,1,1-trichloroethane, were docked in the active site by superimposing a halogenated carbon on C5 of camphor. Thus, the starting geometry for both trajectories was biased in favor of a reactive geometry.

The simulations were done using an all-hydrogen model. Side-chain polar hydrogens were positioned so as to maximize intramolecular hydrogen bonding, using a previously described automated method, NETWORK [33]. The acidic and basic side chains (amino acids aspartic acid, glutamic acid, arginine and lysine), as well as the N- and C-termini were fully charged. In addition, H270 was doubly protonated, based on the favorable hydrogen-bonding pattern found when

both ring nitrogens are donors. We have found that, since this side chain participates in a hydrogen bond between secondary structure elements, a significantly lower deviation from the crystal coordinates is seen if the side chain is fully protonated [33]. In order to compensate for the limited shielding influence afforded by including a 3 Å solvent shell, a distance-dependent dielectric was used. This approach has been successfully used in recent studies of the trp repressor [30]. Inclusion of a relatively small number of explicit waters should have only a small effect on the predictions made, since we are focusing on the dynamics of the buried active site. Some of the advantages and limitations of using a distance-dependent dielectric have been discussed recently [30,34].

The Discover simulation package (Biosym Technologies, v. 2.7) with the consistent valence force field of Hagler and co-workers was used [35,36]. All of the bonded terms, as well as the Lennard-Jones parameters necessary to describe the substrates, were available in the force field release accompanying the Discover 2.7 package. The atomic charges assigned to the substrate are given in Fig. 1 and were calculated by using the default Discover partial charges for the hydrogens and the methyl carbon; charges for the chlorines and the substituted carbon were assigned so as to reproduce the experimental dipole moment of 1,1,1-trichloroethane. The measured gas-phase dipole moment of trichloroethane is 1.78 D [37] and the calculated dipole moment, using the charge set listed in Fig. 1, is 1.79 D. The partial charge determined for chlorine in trichloroethane was used for hexachloroethane as well. The parameters for the heme were identical to those described previously [38].

For each simulation, the system was first minimized for 500 steps with all heavy atoms fixed to relax the added hydrogens. Then the solvent molecules were minimized for 500 steps with the protein heavy atoms fixed. Finally, 1000 steps of minimization were performed with all atoms free to move, to allow any remaining hot spots to relax. The atomic velocities were initialized using a Maxwellian distribution at 50 K, and the system was gradually heated to 300 K over a period of 10 ps. Subsequently, the simulations were continued at 300 K for 140 ps, using a 1.0 fs time step. A constant temperature was maintained by weakly coupling the system to a thermal bath, using the method of Berendsen et al. [39]. Nonbonded interactions were evaluated using a group-based switching function between 9.5 and 11.5 Å and the nonbonded pair list was updated every 20 time steps.

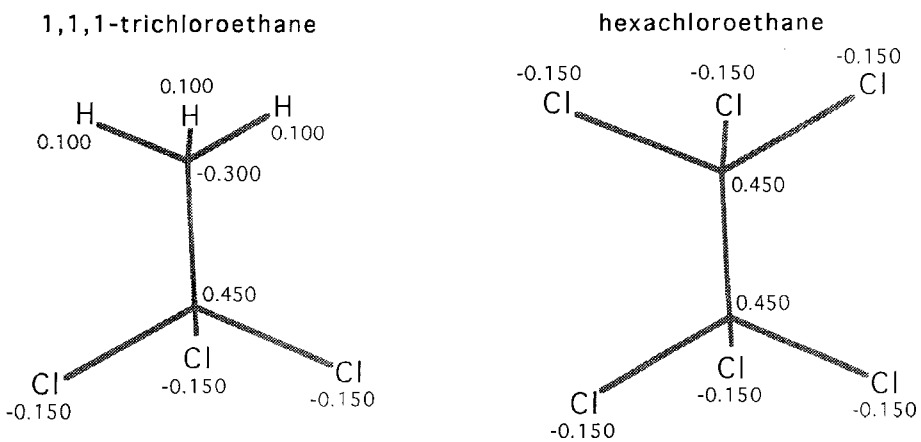

Fig. 1. Partial charges of hexachloroethane and trichloroethane used in this study, in fractions of an electron charge.

RESULTS

Global properties

Before examining in detail the structure and dynamics of the active site of chloroethane-bound cytochrome P450cam, we first monitored several global properties of the enzyme in order to assess the overall stability of the trajectories. These properties included the rms deviation in the position of main-chain atoms with respect to the crystal coordinates, the radius of gyration of the enzyme, the solvent-accessible surface area of the enzyme, and the number of backbone–backbone hydrogen bonds. Minimization alone resulted in an rms deviation for the enzyme heavy atoms of 0.6 Å from the starting coordinates for both the hexachloroethane- and trichloroethane-bound P450cam complexes. During the first 10 ps of each of the trajectories, when the system was being heated to the target temperature, the rms deviation increased an additional 0.8 Å; during the remainder of the trajectories it remained nearly constant. The average values of the rms deviation in protein heavy atom coordinates over the final 130 ps were 1.51 and 1.55 Å for the hexachloroethane- and trichloroethane-bound complexes, respectively. The rms deviation for the main-chain atoms only was approximately 0.2 Å less in both trajectories. These values are slightly lower than those seen in our previous calculations on camphor-bound P450 [38]. However, the present calculations included significantly more explicit solvent than the previously reported camphor-bound simulations, which will tend to keep surface residues closer to their starting positions.

The calculated radius of gyration increased from 21.3 Å for the minimized structure to an average of 21.55 Å for trichloroethane-bound P450 over the final 130 ps, while for hexachloroethane-bound P450 the average was slightly larger, i.e., 21.59 Å. For comparison, the X-ray structure has a calculated radius of gyration of 21.21 Å. The slight increase in the calculated radius of gyration is consistent with the trend seen in our previous P450 trajectories. The solvent-accessible surface area also increased from 16 390 $Å^2$ in the minimized structure to an average of 17 100 ± 100 $Å^2$ over the last 130 ps for both the hexachloro and trichloroethane trajectories. The increase in accessible surface area was due to both the effect of thermal motion and the migration of some of the added solvent into the enzyme. The calculated solvent-accessible surface area in these trajectories was about 10% larger than that calculated for our previous camphor-bound trajectories, which considered crystallographic solvent molecules only and thus had a significantly smaller amount of solvent penetration.

In the minimized structure of trichloroethane-bound P450, there are 202 backbone–backbone hydrogen bonds. During the heating period, this number decreased by 20% because some of the weaker hydrogen bonds were broken by the added thermal energy. Over the final 130 ps, the average number of backbone–backbone hydrogen bonds was 167 ± 6. Of this number, 141 ± 5 were conserved, i.e., also present in the minimized structure. For the hexachloroethane-bound trajectory, these numbers were slightly smaller: 160 ± 6 backbone–backbone hydrogen bonds, 136 ± 5 of which were conserved. The minimized trichloroethane-bound structure contained 139 side-chain hydrogen bonds. Over the last 130 ps, this number averaged 128 ± 5. However, the number of conserved side-chain hydrogen bonds was only 78 ± 4. The hexachloroethane-bound trajectory had the same number of side-chain hydrogen bonds on average, but it contained slightly more conserved hydrogen bonds. The number of backbone–backbone hydrogen bonds in these simulations was very similar to that seen previously for our simulations using a net-neutral model, with

only crystallization waters included. However, the average number of side-chain hydrogen bonds in the present trajectories was about 25% higher than seen in our previous calculations, due to an increase in the number of hydrogen bonds involving ionic side chains.

For each trajectory, an average structure was calculated from the final 130 ps. In Fig. 2, the deviation in C^{α} position from the X-ray coordinates is plotted for each average structure as a function of residue number. The difference between the two time-average structures is shown as well. In general, the deviations between the time-averaged structures and the starting crystal coordinates were small, and the two time-average structures were more similar to each other than either was to the X-ray structure. The mean difference in C^{α} position between the X-ray structure and either time-average structure was 1.0 Å, while that between the two time-average structures was 0.75 Å. The regions of largest deviation between the time-average structure from the trichloroethane-bound trajectory and the X-ray structure included (i) the N- and C-termini; (ii) the turns between helices F and G and between B' and C; (iii) the unstructured region before the start of the L helix; and (iv) interestingly, some of the residues at the start of the J helix. Most of these regions also demonstrated relatively large deviations in the hexachloroethane-bound trajectory. However, the J helix remained much closer to its starting conformation in the hexachloroethane trajectory, while the final turn of the G helix showed significantly larger deviations.

For the residues which line the active-site pocket, i.e., F87, Y96, F98, T185, L244, V247, D251, T252, V295, D297, I395 and V396, the average C^{α} differences between the time-average structure

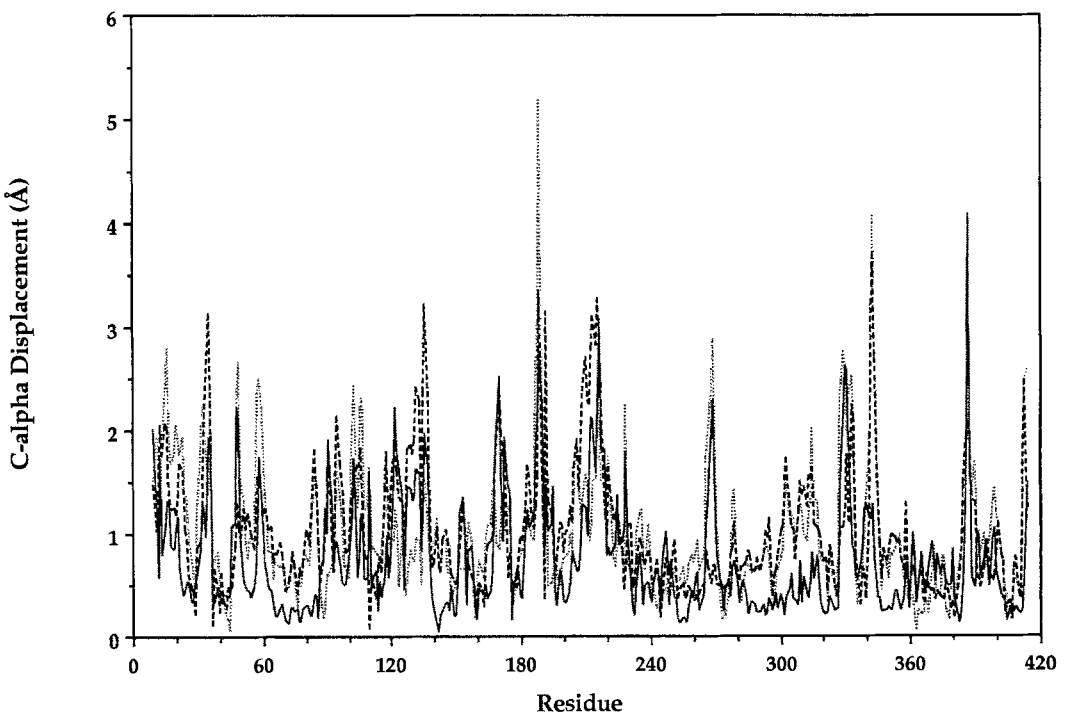

Fig. 2. The deviation in C^{α} position as a function of residue number. The solid line is the deviation between the time-averaged structure of hexachloroethane-bound P450cam and trichloroethane-bound P450cam. The dotted and dashed lines are the differences between the trichloroethane- and hexachloroethane-bound average structures and the X-ray coordinates, respectively.

and the crystal coordinates were 0.67 and 0.90 Å for trichloroethane and hexachloroethane, respectively. These values are slightly smaller than those seen for the protein as a whole. This is to be expected, since many of these active-site residues are part of secondary structure elements and are also generally not very solvent-exposed. The mean difference in C^{α} position for the active-site residues in the two time-averaged structures was 0.63 Å. This difference is again slightly smaller than that seen for the two time-averaged structures as a whole.

In Fig. 3, the calculated heavy-atom rms fluctuations are plotted versus residue number for the final 130 ps of each of the trajectories, as well as the experimentally determined fluctuations for the camphor-bound structure. The average value for the heavy-atom fluctuation was 0.62 Å for both the hexachloro- and trichloroethane trajectories. The corresponding value for the main-chain atoms was 0.55 Å. These values are very similar to those seen in our previous trajectories of P450cam. The pattern of peaks and valleys is similar for all three traces in Fig. 3. However, for most residues, the calculated rms fluctuations are approximately 30% smaller than the experimentally determined values. This may be due in part to the use of a distance-dependent dielectric, which tends to damp atomic fluctuations, as has been noted by others [30,34]. The 10% of the protein with the largest rms fluctuations clusters into two groups; residues in turns between helices, and the N-terminal tail and residues that are in van der Waals contact with this tail. The 10% of the protein with the smallest rms fluctuations is composed of buried residues (the average fraction of the surface area of such residues which is solvent accessible is only 5%, compared to 62% for the most mobile residues) in the helical core of the enzyme.

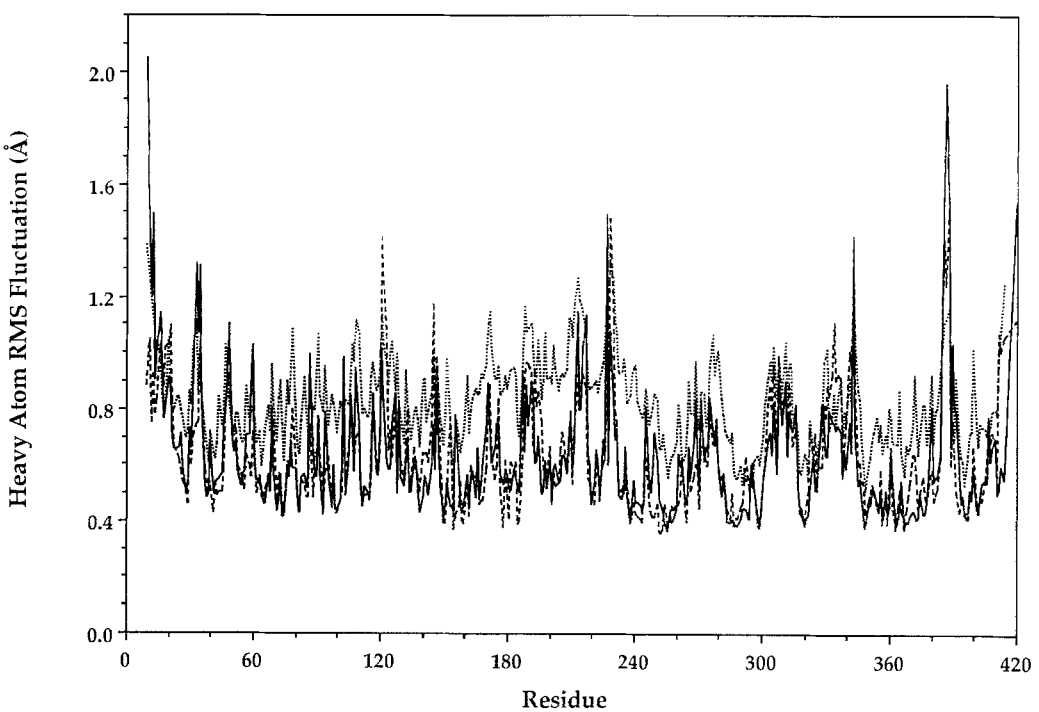

Fig. 3. The rms heavy-atom fluctuation as a function of residue number. The dotted curve represents experimental values, while the solid and dashed curves are for the trichloroethane- and hexachloroethane-bound trajectories, respectively.

In Fig. 4, the rms fluctuations of the backbone dihedral angles ϕ and ψ are plotted as a function of residue number. The mean value for the backbone dihedral angle fluctuations was 12°. This value is similar to that seen in our previous simulations of camphor-bound P450. In both trajectories, only a handful of residues had rms fluctuations greater than 20°. Most of these larger fluctuations are due to crankshaft motion in the turns between helices. The turns between

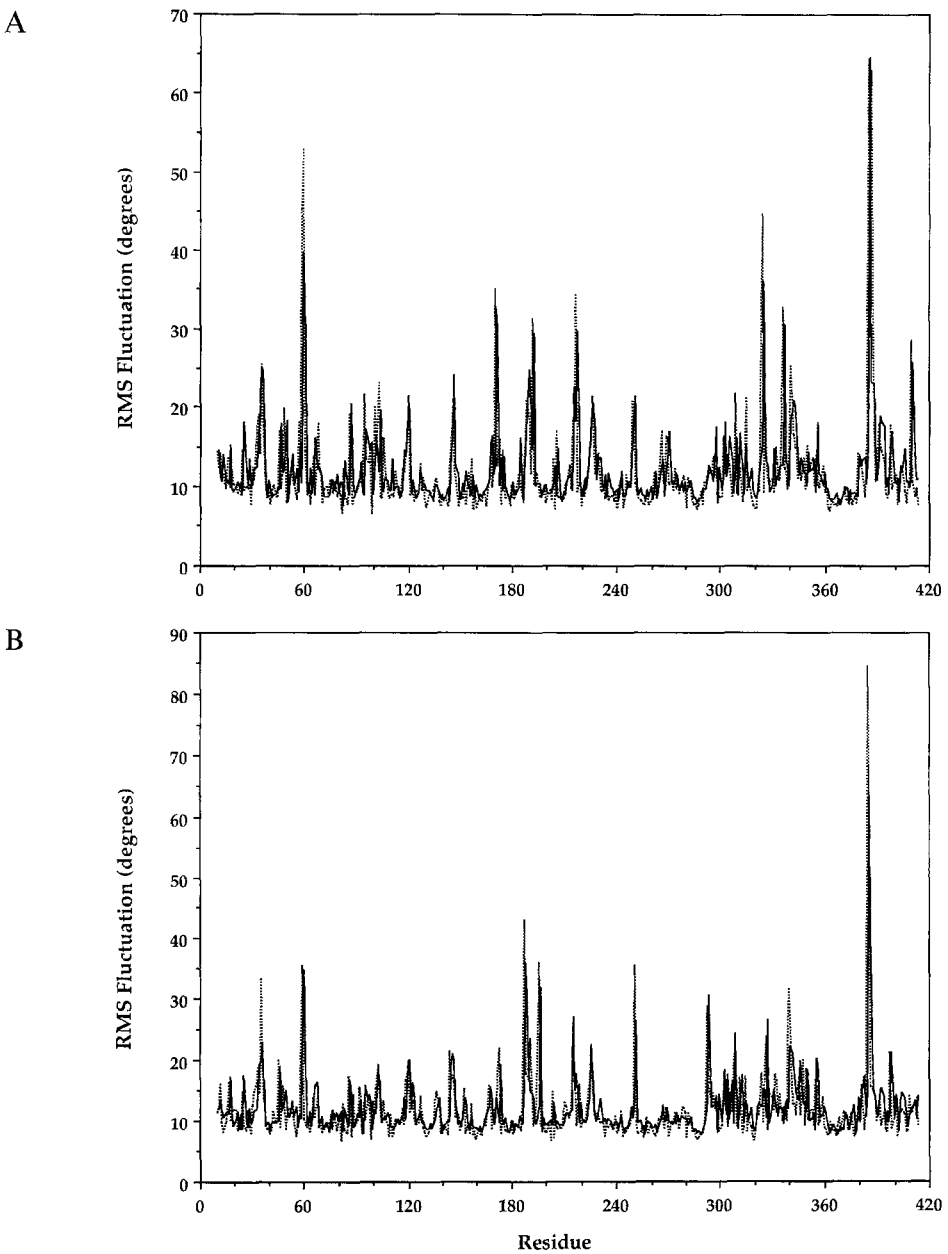

Fig. 4. The rms fluctuation in the backbone dihedral angles ϕ (solid lines) and ψ (dotted lines) as a function of residue number for (A) 1,1,1-trichloroethane-bound P450cam; and (B) hexachloroethane-bound P450cam.

helices D and E, E and F, F and G, and G and H all show this type of behavior. In addition, two regions classified in the X-ray structure as helical show rather large fluctuations, i.e., the region around residues 251–252 in the I helix and the region around residue 120 in the C helix. Both of these regions are actually kinks in their respective helices and have been seen to be highly mobile in several of our previous simulations [38,40]. The unstructured region between residues 336–342 also shows significant backbone motion, and residues 59 to 61 in β-sheet 1 show significant backbone motion in response to movements in the N-terminal region and in the loop between helices F and G.

Active-site motions

One question of interest is the extent to which the active site of cytochrome P450cam repacks to accommodate different substrates. In the crystal structures determined for camphor-bound P450cam and several substrate analogs such as norcamphor, thiocamphor, camphane, adamantane and adamantanone, there is no evidence of any significant repacking in the active site due to variations in substrate volume and shape. However, previous simulations of norcamphor-bound P450 suggested the possibility that for this relatively small substrate, substantial rearrangement in the I helix could occur. In Table 1, the mean values of the dihedral angles ϕ and ψ, calculated from the final 130 ps of the trajectories of hexachloro- and trichloroethane-bound P450cam, are listed for the active-site amino acids (those residues with one or more atoms 4 Å or closer to camphor), along with the corresponding values from the X-ray structure of camphor-bound P450 and the calculated rms fluctuation in these angles. Several backbone dihedral angles show large deviations from the X-ray-determined values. As has been seen in our previous simulations, the kink in the I helix centered around residue T252 is highly mobile [38,40]. The presence of additional explicit solvent in the current simulation did not damp this motion compared to our previous simulations. In addition, the active-site residues in or near the B' helix (F87, Y96 and T101) show large deviations and higher than average fluctuations. The dihedral angles of these residues generally display crankshaft motions and these residues show the largest

TABLE 1
ACTIVE-SITE BACKBONE DIHEDRAL ANGLES FOR TIME-AVERAGED HEXACHLOROETHANE-, 1,1,1-TRICHLOROETHANE- AND CAMPHOR-BOUND P450cam

Residue	ϕ			ψ		
	C_2Cl_6	CCl_3CH_3	X-ray[a]	C_2Cl_6	CCl_3CH_3	X-ray[a]
F87	−97.9 ± 16.6	−92.1 ± 20.4	−102.6	140.8 ± 11.4	133.4 ± 12.8	149.3
Y96	−130.2 ± 15.9	−93.7 ± 17.1	−65.4	110.1 ± 10.1	101.7 ± 13.4	119.4
F98	−61.3 ± 14.2	−76.0 ± 14.5	−61.3	142.4 ± 11.8	122.4 ± 15.4	149.5
T101	−57.0 ± 11.5	−67.5 ± 11.3	−63.4	−39.9 ± 11.1	−10.2 ± 20.1	−32.4
T185	−78.1 ± 10.8	−81.7 ± 16.2	−97.3	−44.3 ± 8.8	−34.9 ± 9.9	−34.5
L244	−66.8 ± 9.1	−69.4 ± 8.8	−69.1	−44.5 ± 7.3	−42.2 ± 7.3	−43.1
V247	−54.7 ± 8.5	−60.2 ± 10.5	−64.2	−47.2 ± 8.4	−48.4 ± 9.8	−44.4
T252	−82.7 ± 26.3	−69.4 ± 11.3	−110.9	−66.7 ± 9.7	−57.6 ± 9.3	−68.5
V295	−85.0 ± 11.9	−88.6 ± 11.4	−107.8	120.4 ± 12.3	126.9 ± 11.4	144.5
D297	−138.4 ± 12.2	−117.7 ± 13.3	−125.3	−162.0 ± 12.1	−166.8 ± 12.7	−161.1
I395	−72.5 ± 9.0	−75.0 ± 9.7	−65.9	−64.8 ± 8.8	−64.5 ± 9.0	−45.6
V396	−99.3 ± 11.6	−97.5 ± 11.1	−123.7	109.3 ± 8.1	114.2 ± 8.4	131.1

[a] Ref. 28.

variability between repeated runs when either camphor or one of the chloroethanes is a substrate. The fact that mobility and conformation in this region seems to be highly variable, even when camphor is the substrate, makes it difficult to determine the effect of different substrates on the dynamic behavior of the active site, but it certainly suggests the possibility that, for substrates either significantly larger or smaller than camphor, substantial rearrangement could occur in the active site.

In contrast to the behavior of the backbone dihedral angles, except for residue F87, the side-chain dihedral angles of all of these active-site residues have small deviations from the X-ray-determined angles, as well as small fluctuations. This is consistent with the trend seen in previous simulations of camphor-, thiocamphor- and norcamphor-bound P450cam [19,38,40]. In the trichloroethane-bound trajectory, both χ^1 and χ^2 of residue 87 are highly mobile, while in the hexachloroethane-bound trajectory only χ^2 shows high mobility. However, in a repeated run of hexachloroethane-bound P450 both side-chain dihedral angles were highly mobile.

In Fig. 5, the time-averaged structure of the active site is superimposed on the X-ray structure. The superpositioning was done using all the heavy atoms of the active-site residues, including the entire heme moiety. The time-averaged structure of hexachloroethane-bound P450 is shown in Fig. 5A, while trichloroethane-bound P450 is shown in Fig. 5B. In both Figs. 5A and B, the movement of the side chain of F87 described above is clearly visible. After the initial heating period, which was not included in the time average, the side chain of F87 spends a considerably larger fraction of the time in its alternate conformation. The rearrangement of the B' helix region described above is also noticeable, while the differences in the I helix region are by comparison quite small.

A second question of both theoretical and experimental interest is the extent to which solvent can enter the active site. For oxidative reactions, excess solvent in the active site is thought to be crucial to uncoupling of product formation from NADH consumption [41]. For the substrates under consideration here, the presence of excess solvent in the active site can alter the extent of spin-state conversion of the heme iron, which is converted from low to high spin upon substrate

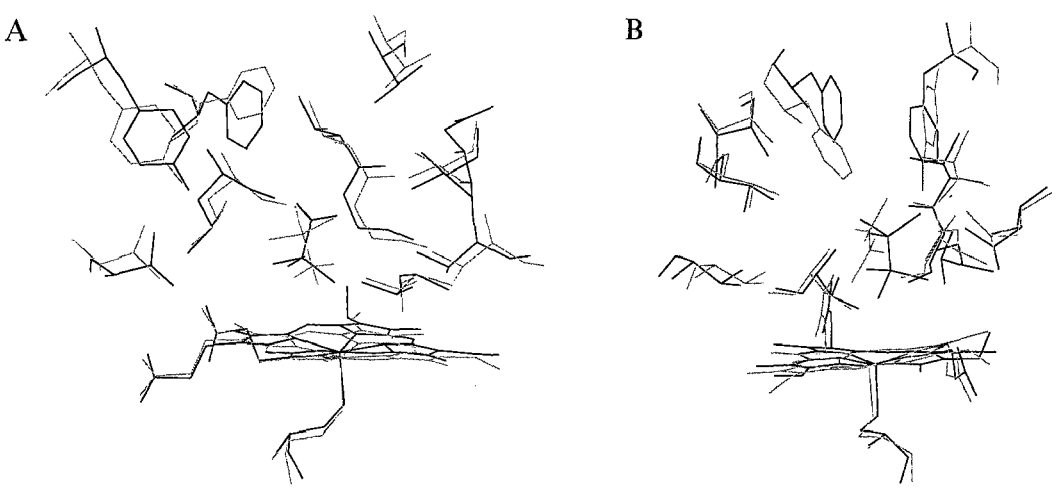

Fig. 5. Superimposed views of the active site of chloroethane-bound cytochrome P450cam for (A) 1,1,1-trichloroethane; and (B) hexachloroethane. The starting structure is shown in black; the time-averaged structure is in gray. For the protein, only the heavy atoms are shown.

binding. An increase in spin-state conversion is coupled to a change in the redox potential of the iron. In a fully low-spin complex, electron transfer from the physiological redox partner is unfavorable, while for a fully high-spin heme iron, the transfer is favorable [42]. In the X-ray structure of camphor-bound P450cam no solvent is observed in the active site, although calculations by Wade suggest there is room for at least four water molecules [43]. In the crystal structures of both norcamphor-bound and thiocamphor-bound P450cam, a single active-site water acts as a distal ligand for the heme iron [44,45]. In the normal oxidative reaction cycle this water is displaced as the distal ligand by O_2, but it remains in the active-site pocket. Previous simulations of camphor-bound P450cam showed no tendency for water to enter the active site [46]. This is perhaps not surprising, considering the limited amount of explicit solvent included in these simulations and the relatively short amount of time simulated. However, in simulations of norcamphor-bound P450cam, crystallographic waters have been observed to enter the active site (M.B. Bass and R.L. Ornstein, unpublished results). Since the substrates under study here are the size of norcamphor or smaller, it is likely that these simulations might also show solvent entering the active site. However, an examination of both trajectories shows only a single solvent molecule within 5.0 Å of the substrate. In both cases this is crystallographic water 652, which in the X-ray structure is part of an ordered solvent channel near the heme propionates. In both simulations it forms an intermittent hydrogen bond with the propionate group of ring A. Although significantly more explicit solvent was used in the present simulations than in our previous simulations of camphor- and norcamphor-bound P450cam, the total length of the trajectories was still too short to allow definitive conclusions about solvent entry into the active site.

In previous simulations of norcamphor-bound P450cam, it was observed that the substrate moved away from the heme iron, so that the average distance from the center of mass of the substrate to the iron was approximately 1.0 Å larger than in the X-ray structure and significantly larger than that observed for the native substrate camphor [40]. The difference in this distance for the two substrates correlates well with the fact that camphor is a highly coupled substrate, while norcamphor is a highly uncoupled substrate. Since both hexachloro- and trichloroethane are substantially smaller than camphor, 30 and 50%, respectively, one might expect both haloethanes to show a similar tendency to move away from the heme. The molecular volumes of hexachloroethane and norcamphor are approximately the same, so there should be ample room for both substrates to either move away from the heme or reorient relative to the heme. For each halosubstrate, the distance of its center of mass to heme iron increased by less than 0.3 Å during the simulation. This result is somewhat surprising, considering the size of the substrates.

In Fig. 6A, the distance from the heme iron to the two carbons of hexachloroethane is plotted as a function of time. A similar plot is shown in Fig. 6B for the trichloroethane trajectory. A comparison of the two trajectories indicates a striking difference in the behavior of the substrates. Hexachloroethane shows very little mobility throughout the simulation. It undergoes no rotations and has a fairly small calculated B-factor, only 34 $Å^2$. In contrast, trichloroethane undergoes a rotation early in the heating phase, which positions the nonhalogenated carbon much closer to the heme iron than the halogenated carbon. After the heating trichloroethane is still quite mobile, with a calculated B-factor of 89 $Å^2$. In the trichloroethane trajectory, fewer than 5% of the snapshots examined have one of the Cl atoms closer than 4.5 Å to the iron. In contrast, more than 95% of the hexachloroethane structures have a Cl atom less than 4.5 Å from the heme iron.

A total of 22 residues plus the heme group spend at least some fraction of the trajectory closer

than 5.5 Å to 1,1,1-trichloroethane. Of these, the heme and 11 residues are within this cutoff during more than two thirds of the trajectory. In Table 2, the average substrate–residue interaction energies and their standard deviations, calculated from the final 140 ps of the trajectory, are shown for these 11 residues, lining the active site for 1,1,1-trichloroethane-bound P450cam. Of the protein residues, V247, L244, F87 and V295, in descending order, interact most favorably

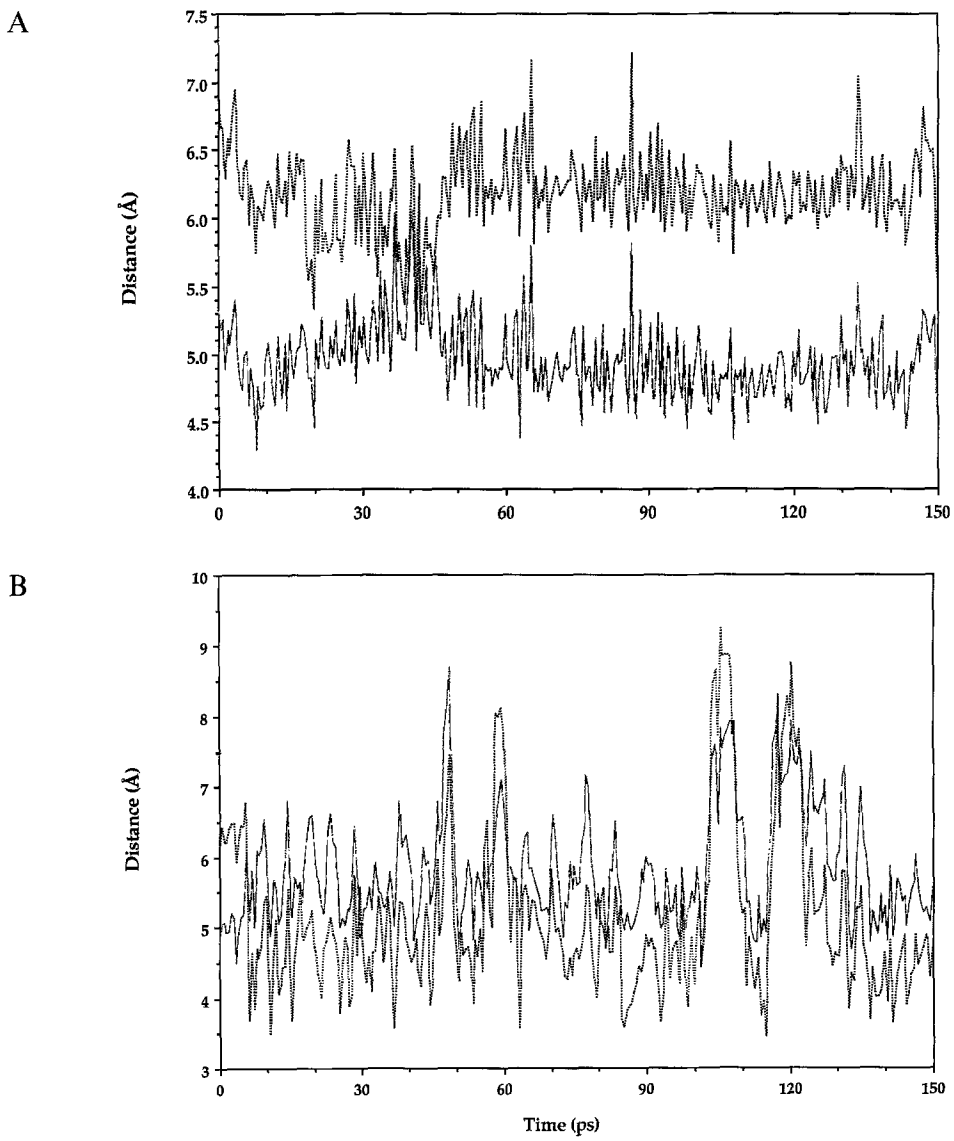

Fig. 6. (A) The distance from the two carbons of hexachloroethane to the heme iron as a function of the time course of the simulation. (B) The corresponding plot for the trichloroethane-bound trajectory. In (B), the thick solid line and the dotted line represent the halogenated carbon and the unsubstituted carbon, respectively. In each plot, the thick solid line monitors the distance between the heme iron and the substrate carbon that is closest to the iron at the start of the simulation.

with 1,1,1-trichloroethane. For these residues the favorable interaction is almost entirely van der Waals in character. However, for 1,1,1-trichloroethane the dominant interaction with the protein is with the heme prosthetic group. The substrate–heme interaction contributes approximately half of the total protein–substrate interaction energy. For hexachloroethane, the interaction with the heme is also the dominant interaction. This interaction comprises a large favorable van der Waals term and a smaller, but unfavorable, Coulombic term. For 1,1,1-trichloroethane, the unfavorable Coulombic term is approximately four times larger than in the case of hexachloroethane. After the rotation of 1,1,1-trichloroethane early in the trajectory, the Coulombic interaction between the substrate and heme group becomes a relatively large favorable interaction. To see whether the observed orientation differences between hexachloroethane and 1,1,1-trichloroethane are not due to the use of a distance-dependent dielectric, we performed the following test. For several time points from the previously calculated trajectories, we performed single-point energy calculations using a constant dielectric of 1. Although the magnitude of the Coulombic interaction between the substrates and the heme changed, the qualitative trend did not.

In order to insure that the difference in the orientation and mobility of the substrates was not an artifact of the initial conditions used in the trajectories, particularly in the case of 1,1,1-trichloroethane, repeated trajectories were calculated for both hexachloro- and trichloroethane-bound P450cam, with either different initial velocities or different choices for the partial charges on the substrate. When a different set of initial velocities was used, the same qualitative behavior was observed for trichloroethane. The substrate rotated very early in the simulation and had a large calculated B-factor. Two alternate charge sets were also examined. In one set the partial charge assigned to a chlorine atom was reduced in magnitude by 25%, with a compensating change in the partial charge of the carbon atom to keep the molecule neutral. In a second trajectory, the partial charge on a chlorine was increased by 50%; this value corresponds to a partial charge appropriate for a monosubstituted chloroethane. With both of these alternate charge sets, the qualitative behavior of the substrate was the same. Repeated trajectories of hexachloroethane with the alternate charge sets also gave qualitatively similar results, a low calculated B-factor relative to trichloroethane, and short Fe-Cl distances in virtually every snapshot examined.

TABLE 2
AVERAGE SUBSTRATE–PROTEIN INTERACTION ENERGIES FOR 1,1,1-TRICHLOROETHANE-BOUND P450cam DURING THE FINAL 140 PS OF AN MD SIMULATION

Residue	Total energy	van der Waals energy	Coulombic energy
F87	−0.77 ± 0.37	−0.69 ± 0.38	−0.08 ± 0.09
Y96	−0.53 ± 0.47	−0.49 ± 0.35	−0.04 ± 0.26
T101	−0.28 ± 0.21	−0.28 ± 0.15	−0.002 ± 0.12
L244	−0.85 ± 0.54	−0.83 ± 0.47	−0.02 ± 0.24
V247	−0.93 ± 0.42	−0.79 ± 0.37	−0.13 ± 0.20
G248	−0.40 ± 0.32	−0.58 ± 0.30	0.17 ± 0.26
T252	−0.27 ± 0.28	−0.39 ± 0.24	0.12 ± 0.21
V295	−0.69 ± 0.43	−0.69 ± 0.46	0.001 ± 0.16
D297	−0.63 ± 0.41	−0.55 ± 0.37	−0.08 ± 0.23
I395	−0.50 ± 0.22	−0.38 ± 0.21	−0.12 ± 0.09
V396	−0.38 ± 0.22	−0.42 ± 0.22	0.04 ± 0.09
Heme	−7.37 ± 2.38	−5.00 ± 1.42	−2.37 ± 1.85

Energies are given in kcal/mol.

DISCUSSION AND CONCLUSIONS

Although the rate of dehalogenation is often very slow, several bacterial enzymes have been shown to dehalogenate organohalides (Refs. 14,47,48 and references cited therein). Wackett and co-workers have recently demonstrated that cytochrome P450cam binds hexachloroethane with a dissociation constant comparable to the binding of the physiological substrate camphor [15]. The enzyme reductively dehalogenates hexachloroethane at a rate that, while two orders of magnitude slower than that estimated for camphor hydroxylation, is significant in comparison to many of the dehalogenation rates reported for anaerobic bacterial cultures. On the other hand, 1,1,1-trichloroethane has a much lower affinity for P450cam and is not dehalogenated under similar conditions. Probably, several factors are responsible for the lack of 1,1,1-trichloroethane dehalogenation. First, substrate reactivity generally decreases with decreasing degree of halogenation. Studies by Loew and co-workers on a series of halogenated methanes show a good correlation between the degree of substitution, the calculated vertical electron affinity and the experimentally observed reactivity of these compounds [49]. A similar correlation between degree of substitution and reactivity is seen for the chlorinated ethanes studied by Wackett and co-workers [15]. In aqueous solution with added hematin, the rate for dechlorination of pentachloroethane is over three orders of magnitude faster than the rate for 1,1,1-trichloroethane (L.P. Wackett, personal communication). This large difference in reactivities is a reflection of the differences in the intrinsic reactivity of the two compounds. However, since there was a measurable rate for dechlorination of 1,1,1-trichloroethane in the presence of hematin, the differences in intrinsic reactivities are not sufficient to completely explain the data of Wackett and co-workers [15].

A second factor contributing to the differing reactivity of hexachloroethane and 1,1,1-trichloroethane is the different ability of the two substrates to bind to P450cam and to induce a change in the spin state of the heme iron. Although P450cam binds 1,1,1-trichloroethane, it shows a much lower affinity than for either hexachloro- or pentachloroethane. The measured value of K_D for trichloroethane is nearly a factor of 60 larger than for pentachloroethane and almost a factor of 600 larger than for hexachloroethane [15]. Furthermore, unlike hexachloroethane, the binding of trichloroethane results in incomplete spin conversion of the heme iron. The ability of a substrate to induce a change in the spin state of the heme iron is directly related to its ability to exclude solvent from the active site. Smaller, more mobile substrates will exclude less solvent, resulting in incomplete conversion of the spin state. While binding of hexachloroethane by P450cam results in more than 95% spin conversion, trichloroethane binding results in only 35% spin conversion. For comparison, the binding of 1,1,1,2-tetrachloroethane, a substrate which is turned over, induces a 50% spin conversion and a rate of product formation that is an order of magnitude slower than that of hexachloroethane [15]. An increase in spin-state conversion from low to high spin shifts the redox potential of the heme iron. In the substrate-free state, the latter has a redox potential which is unfavorable for electron transfer from the physiological redox partner putidaredoxin [42]. For substrates like camphor or hexachloroethane, which induce a nearly complete spin conversion, electron transfer into the heme from putidaredoxin will be enhanced by nearly a factor of 600 compared to the low-spin free enzyme. The observed 35% spin conversion upon binding of trichloroethane results in a redox potential of about –235 mV for the heme iron, based on the linear free-energy relationship between spin conversion and redox potential [42]. Thus, any enhancement in the rate of electron transfer will be modest compared

to a substrate which induces a nearly complete spin conversion. For comparison, binding of the substrate analog norcamphor shifts the redox potential of the heme iron to –206 mV, and results in a 34-fold increase in the rate of electron transfer, compared to the free enzyme [42].

Our simulations suggest a third factor contributing to the lack of turnover of 1,1,1-trichloroethane by P450cam, i.e., the fact that the preferred substrate orientation in the active site and the high mobility of the substrate are both unfavorable for dehalogenation. For hexachloroethane, a single chlorine atom is close to van der Waals contact with the heme iron for virtually the entire simulation. In contrast, trichloroethane has high mobility, which should disfavor reactivity, and its preferred conformation has the substituted carbon far from the heme iron. These observations are consistent with the experimentally observed differences between nonenzymatic dechlorination in the presence of hematin and enzymatic dechlorination by P450cam. While the presence of cytochrome P450cam results in a 100-fold enhancement of the dechlorination rate for pentachloroethane over that seen in hematin solution, presumably due to a proximity effect, the dechlorination rate for 1,1,1-trichloroethane is actually decreased beyond the detection limit of the experiment in the presence of P450cam. The relative rates of dechlorination for the two substrates in the presence of P450cam are at least six orders of magnitude different, in contrast to the three orders of magnitude difference in aqueous solutions containing hematin.

We are currently attempting to redesign the active site of P450cam, in order to facilitate dehalogenation of 1,1,1,-trichloroethane. One approach that we are currently exploring is to repack active-site residues that only weakly interact with the substrate. Presumably, by altering the shape of such residues to enhance the favorable substrate–enzyme interaction, while favoring a configuration that allows for appropriate orbital interaction of iron and chlorine, the K_D should be reduced, the spin conversion increased, the substrate mobility reduced and the reactivity for dechlorination increased.

ACKNOWLEDGEMENTS

We thank Professor Lawrence Wackett for access to unpublished data and Professors Wackett and Steve Sligar for fruitful discussions. Pacific Northwest Laboratory is operated for the U.S. Department of Energy by the Battelle Memorial Institute under Contract DE-AC06-76RLO 1830. This work was supported by grant KP0402 from the Health Effects and Life Sciences Research Division of the Office of Health and Environmental Research of the U.S. Department of Energy (R.L.O.).

REFERENCES

1 Riley, R.G., Zachara, J.M. and Wobber, F.J., Chemical Contaminants on DOE Lands and Selection of Contaminant Mixtures for Subsurface Science Research, Report no. DE92-014826, U.S. Department of Energy, 1992.
2 Guengerich, F.P., J. Biol. Chem., 266 (1991) 10019.
3 Walsh, C., Enzymatic Reaction Mechanisms, Freeman, San Francisco, CA, 1979.
4 Ortiz de Montellano, P.R., In Ortiz de Montellano, P.R. (Ed.) Cytochrome P450: Structure, Mechanism and Biochemistry, Plenum, New York, NY, 1986, pp. 217–271.
5 Nebert, D.W. and Gonzales, F.J., Annu. Rev. Biochem., 56 (1987) 945.
6 Macdonald, T.L., Crit. Rev. Toxicol., 11 (1983) 85.
7 Anders, M.W. and Pohl, L.R., In Anders, M.W. (Ed.) Bioactivation of Foreign Compounds, Academic Press, Orlando, FL, 1985, pp. 283–315.

8 Castro, C.E., Wade, R.S. and Belser, N.O., Biochemistry, 24 (1985) 204.
9 Castro, C.E., Yokoyama, W. and Belser, N.O., Environ. Toxicol. Chem., 8 (1989) 13.
10 Lam, T. and Vilker, V.L., Biotechnol. Bioeng., 24 (1987) 151.
11 Miller, R.E. and Guengerich, F.P., Biochemistry, 21 (1982) 1090.
12 Miller, R.E. and Guengerich, F.P., Cancer Res., 43 (1983) 1145.
13 Vilker, V.L. and Khan, F., Biotechnol. Prog., 5 (1989) 70.
14 Wackett, L.P., Logan, M.S.P. and Blocki, F.A., Biodegradation, 3 (1992) 19.
15 Logan, M.S.P., Newman, L.M., Schanke, C.A. and Wackett, L.P., Biodegradation, 4 (1993) 39.
16 Sligar, S.G. and Murray, R.I., In Ortiz de Montellano, P.R. (Ed.) Cytochrome P450: Structure, Mechanism and Biochemistry, Plenum, New York, NY, 1986, pp. 429–503.
17 Poulos, T.L. and Raag, R., FASEB J., 6 (1992) 674.
18 Paulsen, M.D. and Ornstein, R.L., J. Comput.-Aided Mol. Design, 6 (1992) 449.
19 Paulsen, M.D. and Ornstein, R.L., Protein Eng., 6 (1993) 359.
20 Filipovic, D., Paulsen, M.D., Loida, P., Ornstein, R.L. and Sligar, S.G., Biochem. Biophys. Res. Commun., 189 (1992) 488.
21 Fruetel, J.A., Collins, J.R., Camper, D.L., Loew, G.H. and Ortiz de Montellano, P.R., J. Am. Chem. Soc., 114 (1992) 6987.
22 Ortiz de Montellano, P.R., Fruetel, J.A., Collins, J.R., Camper, D.L. and Loew, G.H., J. Am. Chem. Soc., 113 (1991) 3195.
23 Collins, J.R., Camper, D.L. and Loew, G.H., J. Am. Chem. Soc., 113 (1991) 2736.
24 Jones, J.P., Trager, W.F. and Carlson, T.J., J. Am. Chem. Soc., 115 (1993) 381.
25 Sligar, S.G., Filipovic, D. and Stayton, P.S., Methods Enzymol., 206 (1991) 31.
26 Paulsen, M.D., Filipovic, D., Sligar, S.G. and Ornstein, R.L., Protein Sci., 2 (1993) 357.
27 Loida, P.J. and Sligar, S.G., Protein Eng., 6 (1993) 207.
28 Poulos, T.L., Finzel, B.C. and Howard, A.J., J. Mol. Biol., 195 (1987) 687.
29 Bernstein, F.C., Koetzle, T.F., Williams, G.J.B., Meyer Jr., E.F., Brice, M.D., Rodgers, J.R., Kennard, O., Shimanouchi, T. and Tasumi, M., J. Mol. Biol., 112 (1977) 535.
30 Guenot, J. and Kollman, P.A., Protein Sci., 1 (1992) 1185.
31 Steinbach, P.J., Loncharich, R.J. and Brooks, B.R., Chem. Phys., 158 (1991) 383.
32 DiPrimo, C., Hui Bon Hua, G., Douzou, P. and Sligar, S.G., Eur. J. Biochem., 193 (1990) 383.
33 Bass, M.B., Hopkins, D.F., Jaquyash, W.A.N. and Ornstein, R.L., Protein Struct. Funct. Genet., 12 (1992) 266.
34 Arnold, G.E. and Ornstein, R.L., Protein Struct. Funct. Genet., 18 (1994) 1.
35 Hagler, A.T., In Hruby, V.J. and Meienhofer, J. (Eds.) The Peptides, Academic Press, New York, NY, 1985, pp. 213–299.
36 Dauber-Osguthorpe, P., Roberts, V.A., Osguthorpe, D.J., Wolff, J., Genest, M. and Hagler, A.T., Protein Struct. Funct. Genet., 4 (1988) 31.
37 Weast, R.C. (Ed.) Handbook of Chemistry and Physics, 56th ed., CRC Press, Boca Raton, FL, 1975, p. E64.
38 Paulsen, M.D. and Ornstein, R.L., Protein Struct. Funct. Genet., 11 (1991) 184.
39 Berendsen, H.J.C., Postma, J.P.M., Van Gunsteren, W.F., DiNola, A. and Haak, J.R., J. Chem. Phys., 81 (1984) 3684.
40 Bass, M.B., Paulsen, M.D. and Ornstein, R.L., Protein Struct. Funct. Genet., 13 (1992) 26.
41 Atkins, W.M. and Sligar, S.G., J. Am. Chem. Soc., 109 (1987) 3754.
42 Fisher, M.T. and Sligar, S.G., J. Am. Chem. Soc., 107 (1985) 5018.
43 Wade, R.C., J. Comput.-Aided Mol. Design, 4 (1990) 199.
44 Raag, R. and Poulos, T.L., Biochemistry, 28 (1989) 917.
45 Raag, R. and Poulos, T.L., Biochemistry, 30 (1991) 2674.
46 Paulsen, M.D., Bass, M.B. and Ornstein, R.L., J. Biomol. Struct. Dyn., 9 (1991) 187.
47 Gantzer, C.J. and Wackett, L.P., Environ. Sci. Technol., 25 (1991) 715.
48 Schanke, C.A. and Wackett, L.P., Environ. Sci. Technol., 26 (1992) 830.
49 Luke, B.T., Loew, G.H. and McLean, A.D., J. Am. Chem. Soc., 110 (1988) 3396.